

First observation of PeV-energy neutrinos with IceCube

M. G. Aartsen,² R. Abbasi,²⁷ Y. Abdou,²² M. Ackermann,⁴¹ J. Adams,¹⁵ J. A. Aguilar,²¹ M. Ahlers,²⁷ D. Altmann,⁹ J. Auffenberg,²⁷ X. Bai,^{31,*} M. Baker,²⁷ S. W. Barwick,²³ V. Baum,²⁸ R. Bay,⁷ J. J. Beatty,^{17,18} S. Bechet,¹² J. Becker Tjus,¹⁰ K.-H. Becker,⁴⁰ M. Bell,³⁸ M. L. Benabderrahmane,⁴¹ S. BenZvi,²⁷ J. Berdermann,⁴¹ P. Berghaus,⁴¹ D. Berley,¹⁶ E. Bernardini,⁴¹ A. Bernhard,³⁰ D. Bertrand,¹² D. Z. Besson,²⁵ G. Binder,^{8,7} D. Bindig,⁴⁰ M. Bissok,¹ E. Blaufuss,¹⁶ J. Blumenthal,¹ D. J. Boersma,³⁹ S. Bohachuk,²⁰ C. Boehm,³⁴ D. Bose,¹³ S. Böser,¹¹ O. Botner,³⁹ L. Brayeur,¹³ H.-P. Bretz,⁴¹ A. M. Brown,¹⁵ R. Bruijn,²⁴ J. Brunner,⁴¹ M. Carson,²² J. Casey,⁵ M. Casier,¹³ D. Chirkin,²⁷ A. Christov,²¹ B. Christy,¹⁶ K. Clark,³⁸ F. Clevermann,¹⁹ S. Coenders,¹ S. Cohen,²⁴ D. F. Cowen,^{38,37} A. H. Cruz Silva,⁴¹ M. Danninger,³⁴ J. Daughhetee,⁵ J. C. Davis,¹⁷ C. De Clercq,¹³ S. De Ridder,²² P. Desiati,²⁷ M. de With,⁹ T. DeYoung,³⁸ J. C. Díaz-Vélez,²⁷ M. Dunkman,³⁸ R. Eagan,³⁸ B. Eberhardt,²⁸ J. Eisch,²⁷ R. W. Ellsworth,¹⁶ S. Euler,¹ P. A. Evenson,³¹ O. Fadiran,²⁷ A. R. Fazely,⁶ A. Fedynitch,¹⁰ J. Feintzeig,²⁷ T. Feusels,²² K. Filimonov,⁷ C. Finley,³⁴ T. Fischer-Wasels,⁴⁰ S. Flis,³⁴ A. Franckowiak,¹¹ R. Franke,⁴¹ K. Frantzen,¹⁹ T. Fuchs,¹⁹ T. K. Gaisser,³¹ J. Gallagher,²⁶ L. Gerhardt,^{8,7} L. Gladstone,²⁷ T. Glüsenkamp,⁴¹ A. Goldschmidt,⁸ G. Golup,¹³ J. G. Gonzalez,³¹ J. A. Goodman,¹⁶ D. Góra,⁴¹ D. Grant,²⁰ A. Groß,³⁰ M. Gurtner,⁴⁰ C. Ha,^{8,7} A. Haj Ismail,²² P. Hallen,¹ A. Hallgren,³⁹ F. Halzen,²⁷ K. Hanson,¹² D. Heereman,¹² D. Heinen,¹ K. Helbing,⁴⁰ R. Hellauer,¹⁶ S. Hickford,¹⁵ G. C. Hill,² K. D. Hoffman,¹⁶ R. Hoffmann,⁴⁰ A. Homeier,¹¹ K. Hoshina,²⁷ W. Huelsnitz,^{16,†} P. O. Hulth,³⁴ K. Hultqvist,³⁴ S. Hussain,³¹ A. Ishihara,^{14,‡} E. Jacobi,⁴¹ J. Jacobsen,²⁷ K. Jagielski,¹ G. S. Japaridze,⁴ K. Jero,²⁷ O. Jlelati,²² B. Kaminsky,⁴¹ A. Kappes,⁹ T. Karg,⁴¹ A. Karle,²⁷ J. L. Kelley,²⁷ J. Kiryluk,³⁵ F. Kislat,⁴¹ J. Kläs,⁴⁰ S. R. Klein,^{8,7} J.-H. Köhne,¹⁹ G. Kohnen,²⁹ H. Kolanoski,⁹ L. Köpke,²⁸ C. Kopper,²⁷ S. Kopper,⁴⁰ D. J. Koskinen,³⁸ M. Kowalski,¹¹ M. Krasberg,²⁷ K. Krings,¹ G. Kroll,²⁸ J. Kunnen,¹³ N. Kurahashi,²⁷ T. Kuwabara,³¹ M. Labare,¹³ H. Landsman,²⁷ M. J. Larson,³⁶ M. Lesiak-Bzdak,³⁵ M. Leuermann,¹ J. Leute,³⁰ J. Lünemann,²⁸ J. Madsen,³³ R. Maruyama,²⁷ K. Mase,¹⁴ H. S. Matis,⁸ F. McNally,²⁷ K. Meagher,¹⁶ M. Merck,²⁷ P. Mészáros,^{37,38} T. Meures,¹² S. Miarecki,^{8,7} E. Middell,⁴¹ N. Milke,¹⁹ J. Miller,¹³ L. Mohrmann,⁴¹ T. Montaruli,^{21,§} R. Morse,²⁷ R. Nahnauer,⁴¹ U. Naumann,⁴⁰ H. Niederhausen,³⁵ S. C. Nowicki,²⁰ D. R. Nygren,⁸ A. Obertacke,⁴⁰ S. Odrowski,³⁰ A. Olivas,¹⁶ M. Olivo,¹⁰ A. O’Murchadha,¹² L. Paul,¹ J. A. Pepper,³⁶ C. Pérez de los Heros,³⁹ C. Pfendner,¹⁷ D. Pieloth,¹⁹ E. Pinat,¹² N. Pirk,⁴¹ J. Posselt,⁴⁰ P. B. Price,⁷ G. T. Przybylski,⁸ L. Rädcl,¹ M. Rameez,²¹ K. Rawlins,³ P. Redl,¹⁶ R. Reimann,¹ E. Resconi,³⁰ W. Rhode,¹⁹ M. Ribordy,²⁴ M. Richman,¹⁶ B. Riedel,²⁷ J. P. Rodrigues,²⁷ C. Rott,^{17,¶} T. Ruhe,¹⁹ B. Ruzybayev,³¹ D. Ryckbosch,²² S. M. Saba,¹⁰ T. Salameh,³⁸ H.-G. Sander,²⁸ M. Santander,²⁷ S. Sarkar,³² K. Schatto,²⁸ M. Scheel,¹ F. Scheriau,¹⁹ T. Schmidt,¹⁶ M. Schmitz,¹⁹ S. Schoenen,¹ S. Schöneberg,¹⁰ A. Schönwald,⁴¹ A. Schukraft,¹ L. Schulte,¹¹ O. Schulz,³⁰ D. Seckel,³¹ Y. Sestayo,³⁰ S. Seunarine,³³ C. Sheremata,²⁰ M. W. E. Smith,³⁸ M. Soiron,¹ D. Soldin,⁴⁰ G. M. Spiczak,³³ C. Spiering,⁴¹ M. Stamatikos,^{17,**} T. Stanev,³¹ A. Stasik,¹¹ T. Stezelberger,⁸ R. G. Stokstad,⁸ A. Stöbl,⁴¹ E. A. Strahler,¹³ R. Ström,³⁹ G. W. Sullivan,¹⁶ H. Taavola,³⁹ I. Taboada,⁵ A. Tamburro,³¹ S. Ter-Antonyan,⁶ G. Tešić,³⁸ S. Tilav,³¹ P. A. Toale,³⁶ S. Toscano,²⁷ M. Usner,¹¹ D. van der Drift,^{8,7} N. van Eijndhoven,¹³ A. Van Overloop,²² J. van Santen,²⁷ M. Vehring,¹ M. Voge,¹¹ M. Vraeghe,²² C. Walck,³⁴ T. Waldenmaier,⁹ M. Wallraff,¹ R. Wasserman,³⁸ Ch. Weaver,²⁷ M. Wellons,²⁷ C. Wendt,²⁷ S. Westerhoff,²⁷ N. Whitehorn,²⁷ K. Wiebe,²⁸ C. H. Wiebusch,¹ D. R. Williams,³⁶ H. Wissing,¹⁶ M. Wolf,³⁴ T. R. Wood,²⁰ K. Woschnagg,⁷ C. Xu,³¹ D. L. Xu,³⁶ X. W. Xu,⁶ J. P. Yanez,⁴¹ G. Yodh,²³ S. Yoshida,¹⁴ P. Zarzhitsky,³⁶ J. Ziemann,¹⁹ S. Zierke,¹ A. Zilles,¹ and M. Zoll³⁴

(IceCube Collaboration)

¹*III. Physikalisches Institut, RWTH Aachen University, D-52056 Aachen, Germany*

²*School of Chemistry & Physics, University of Adelaide, Adelaide SA, 5005 Australia*

³*Dept. of Physics and Astronomy, University of Alaska Anchorage, 3211 Providence Dr., Anchorage, AK 99508, USA*

⁴*CTSPS, Clark-Atlanta University, Atlanta, GA 30314, USA*

⁵*School of Physics and Center for Relativistic Astrophysics, Georgia Institute of Technology, Atlanta, GA 30332, USA*

⁶*Dept. of Physics, Southern University, Baton Rouge, LA 70813, USA*

⁷*Dept. of Physics, University of California, Berkeley, CA 94720, USA*

⁸*Lawrence Berkeley National Laboratory, Berkeley, CA 94720, USA*

⁹*Institut für Physik, Humboldt-Universität zu Berlin, D-12489 Berlin, Germany*

¹⁰*Fakultät für Physik & Astronomie, Ruhr-Universität Bochum, D-44780 Bochum, Germany*

¹¹*Physikalisches Institut, Universität Bonn, Nussallee 12, D-53115 Bonn, Germany*

- ¹²*Université Libre de Bruxelles, Science Faculty CP230, B-1050 Brussels, Belgium*
¹³*Vrije Universiteit Brussel, Dienst ELEM, B-1050 Brussels, Belgium*
¹⁴*Dept. of Physics, Chiba University, Chiba 263-8522, Japan*
¹⁵*Dept. of Physics and Astronomy, University of Canterbury, Private Bag 4800, Christchurch, New Zealand*
¹⁶*Dept. of Physics, University of Maryland, College Park, MD 20742, USA*
¹⁷*Dept. of Physics and Center for Cosmology and Astro-Particle Physics, Ohio State University, Columbus, OH 43210, USA*
¹⁸*Dept. of Astronomy, Ohio State University, Columbus, OH 43210, USA*
¹⁹*Dept. of Physics, TU Dortmund University, D-44221 Dortmund, Germany*
²⁰*Dept. of Physics, University of Alberta, Edmonton, Alberta, Canada T6G 2E1*
²¹*Département de physique nucléaire et corpusculaire, Université de Genève, CH-1211 Genève, Switzerland*
²²*Dept. of Physics and Astronomy, University of Gent, B-9000 Gent, Belgium*
²³*Dept. of Physics and Astronomy, University of California, Irvine, CA 92697, USA*
²⁴*Laboratory for High Energy Physics, École Polytechnique Fédérale, CH-1015 Lausanne, Switzerland*
²⁵*Dept. of Physics and Astronomy, University of Kansas, Lawrence, KS 66045, USA*
²⁶*Dept. of Astronomy, University of Wisconsin, Madison, WI 53706, USA*
²⁷*Dept. of Physics and Wisconsin IceCube Particle Astrophysics Center, University of Wisconsin, Madison, WI 53706, USA*
²⁸*Institute of Physics, University of Mainz, Staudinger Weg 7, D-55099 Mainz, Germany*
²⁹*Université de Mons, 7000 Mons, Belgium*
³⁰*T.U. Munich, D-85748 Garching, Germany*
³¹*Bartol Research Institute and Department of Physics and Astronomy, University of Delaware, Newark, DE 19716, USA*
³²*Dept. of Physics, University of Oxford, 1 Keble Road, Oxford OX1 3NP, UK*
³³*Dept. of Physics, University of Wisconsin, River Falls, WI 54022, USA*
³⁴*Oskar Klein Centre and Dept. of Physics, Stockholm University, SE-10691 Stockholm, Sweden*
³⁵*Department of Physics and Astronomy, Stony Brook University, Stony Brook, NY 11794-3800, USA*
³⁶*Dept. of Physics and Astronomy, University of Alabama, Tuscaloosa, AL 35487, USA*
³⁷*Dept. of Astronomy and Astrophysics, Pennsylvania State University, University Park, PA 16802, USA*
³⁸*Dept. of Physics, Pennsylvania State University, University Park, PA 16802, USA*
³⁹*Dept. of Physics and Astronomy, Uppsala University, Box 516, S-75120 Uppsala, Sweden*
⁴⁰*Dept. of Physics, University of Wuppertal, D-42119 Wuppertal, Germany*
⁴¹*DESY, D-15735 Zeuthen, Germany*

(Dated: May 4, 2019)

We report on the observation of two neutrino-induced events which have an estimated deposited energy in the IceCube detector of 1.04 ± 0.16 and 1.14 ± 0.17 PeV, respectively, the highest neutrino energies observed so far. These events are consistent with fully contained particle showers induced by neutral-current $\nu_{e,\mu,\tau}$ ($\bar{\nu}_{e,\mu,\tau}$) or charged-current ν_e ($\bar{\nu}_e$) interactions within the IceCube detector. The events were discovered in a search for ultra-high energy neutrinos using data corresponding to 615.9 days effective livetime. The two neutrino events are observed over an expected atmospheric background of 0.082 ± 0.004 (stat) $^{+0.041}_{-0.057}$ (syst). The resulting p-value for the background-only hypothesis is 2.9×10^{-3} (2.8σ) taking into account the uncertainty on the expected number of background events. Though the two events could be a first indication of an astrophysical neutrino flux, the moderate significance and the uncertainties on the expected atmospheric background from neutrinos produced in the decay of charmed mesons do not allow for a firm conclusion at this point.

PACS numbers: 98.70.Sa, 95.55.Vj

Astrophysical neutrinos are key probes of the high-energy universe. Because of their unique properties, neutrinos escape even dense regions, are undeflected in galactic or extra-galactic magnetic fields and traverse the photon-filled universe unhindered. Thus, neutrinos provide direct information about the dynamics and interiors of extra-ordinary objects in deep space like gamma-ray bursts and active galactic nuclei. Neutrinos at energies above several 100 TeV are particularly interesting as the atmospheric background in this region is very low and a few astrophysical neutrinos can be significant. This let-

ter reports on the observation of two high-energy particle shower events discovered in a search for ultra-high energy neutrinos above about 1 PeV using the IceCube detector.

IceCube [1] detects and reconstructs neutrinos by recording Cherenkov photons emitted from secondary charged particles produced in neutral-current (NC) or charged-current (CC) interactions of the neutrinos in the 2,800 m thick glacial ice at the geographic South Pole. IceCube construction started in 2005 and was completed in December 2010. The detector consists of an array

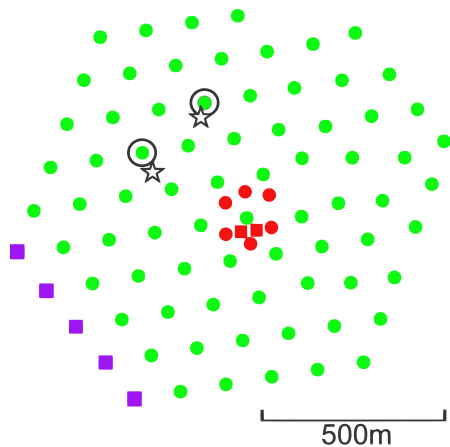


FIG. 1. Surface view of the full IceCube (IC86) detector layout. Filled marks represent the x - y positions of the IceCube strings. Red marks in the central region are the DeepCore strings. Squares represent the strings that did not exist in the IC79 configuration. Open circles are the positions of the closest strings to the observed two cascade events. Stars are the reconstructed vertex positions of the two cascade events.

of 5,160 optical sensors (digital optical modules, DOMs) on 86 strings at depths between 1,450m and 2,450m that instrument a volume of 1 km^3 of ice. Eight out of the 86 strings belong to the DeepCore sub-array [2], a more densely instrumented volume in the bottom center of the detector. Each DOM consists of a 10" photomultiplier tube (PMT) that is protected from the high pressure of the ice by a glass sphere that also contains electronics to amplify and digitize the pulses [3] from the PMTs [4]. Events are recorded as a series of pulses (waveform) in each DOM where one can distinguish between two basic neutrino event signatures: a track-like light pattern in the detector originating from neutrino-induced muons (tracks) and a spherical light pattern produced by hadronic or electromagnetic particle showers (cascades). If not explicitly mentioned, we do not distinguish between neutrinos and anti-neutrinos here.

The analysis selects neutrino candidates calorimetrically using the total number of observed photo-electrons in each event (NPE) as a proxy of the deposited energy [5], thus retaining both bright tracks and cascades. Background events for this analysis are induced by muons and neutrinos generated in interactions of cosmic-rays in the atmosphere. Because of their steeply falling energy spectra, little background is expected in the signal region above 1 PeV. The zenith angle distribution of atmospheric muons peaks in the downward-going direction and sharply decreases towards the horizon with a cut-off at a zenith angle θ of $\cos \theta \approx 0.15$ due to absorption in the Earth, while the atmospheric neutrino distributions have a weaker zenith-angle dependence. In addition to a global lower cut on NPE, the analysis rejects downward-going atmospheric muons by employing event reconstruc-

tions based on a track hypothesis in combination with a higher NPE cut in the downward-going region. All remaining events above the combined NPE threshold are considered to be signal candidates independent of their topological properties.

Data were collected between May 2010 and May 2012, an effective livetime of 615.9 days excluding 54.2 days used for the optimization of the analysis. From May 2010 to May 2011, DOMs on 79 strings (IC79) were operational. This IC79 run period was immediately followed by the first year of data taking with the full 86-string (IC86) detector that lasted until May 2012. The layout of the IC86 configuration is shown in Fig. 1. Events are triggered when eight or more DOMs record signals in local coincidences. Such a coincidence occurs when a nearest or next-to-nearest DOM on the same string triggers within $\pm 1\ \mu\text{s}$ [3].

The collected data are filtered at the South Pole with a condition $\text{NPE} \geq 1000$, and then sent to a northern computer farm via satellite. In order to avoid biases, only about 10% of the data was used to develop the event selection. Photo-electron arrival times are extracted from each waveform and stored as "hits". To remove random coincident noise hits, a two-staged hit cleaning based on the spatial distance and the time interval between hits is applied. Data from the DeepCore strings is discarded to maintain uniformity across the detector volume. To reject dominant downward-going atmospheric muon background, only events with at least 300 hits and $\text{NPE} \geq 3200$ are retained and their directions are reconstructed with a track hypothesis. For the IC79 sample, a log-likelihood (LLH) fit of a muon-track hypothesis based on probability distributions of the photon arrival times at each DOM is performed [9]. A loose cut on a fit quality parameter is applied to filter out events which contain muons from independent air showers. For the IC86 sample, a robust regression technique [10, 11] is utilized to remove hits that have a timing significantly different from what is expected from the bulk of the photon signal from a muon track. Afterwards, the particle directions are reconstructed using the LineFit algorithm [5]. These algorithms are designed to reconstruct muon track events with a zenith angle resolution of 1° or better. For cascade events which resemble point-like light sources, the reconstruction behavior is quite different, and the track reconstruction finds nearly arbitrary zenith angles. However, there is a tendency toward upward-going and horizontal directions for the LLH fit and LineFit respectively. Since for these directions the NPE cut is lower than for downward-going events (see Fig. 2 and Eq. 1), such events can be retained in the final sample even if they would be rejected on account of their true direction.

The final-level selection criteria are based on Monte Carlo simulations of background and signal events. They are determined by optimizing the NPE-threshold values for each of the IC79 and IC86 samples to discover a sig-

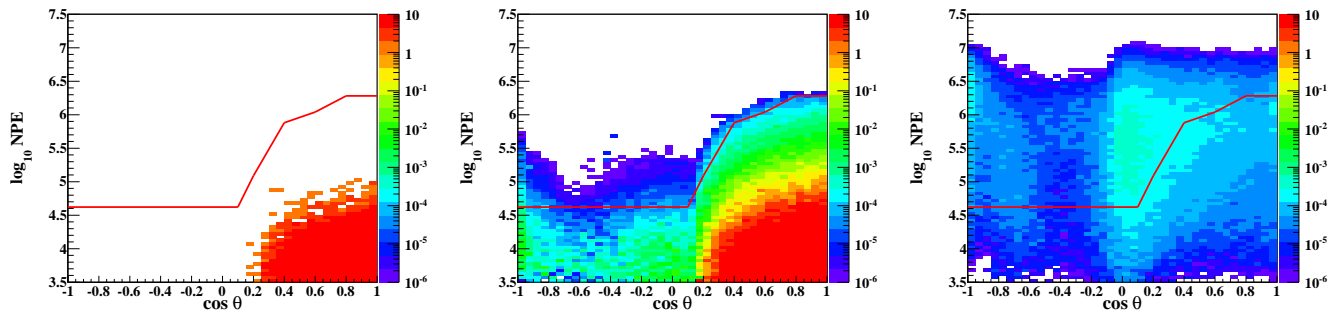


FIG. 2. Distribution of NPE and reconstructed zenith angle for the IC79 events. The experimental test sample is shown in the left panel. The total background (middle panel) and cosmogenic signal neutrino Monte Carlo [6] (right panel) are also displayed. The colors show event numbers per livetime of 33.4 days for the IC79 test sample. The signal distribution contains all three neutrino flavors. The background distributions include atmospheric muons from the CORSIKA package [7] with the SIBYLL high-energy interaction model [8] assuming pure iron primary composition, conventional atmospheric neutrinos, and prompt atmospheric neutrinos. The solid lines in each panel represent the final selection criteria for IC79.

nal [12, 13] from the cosmogenic neutrino model [6]. Figure 2 shows the event distributions for the Monte Carlo simulations and the 10% experimental IC79 test sample corresponding to a livetime of 33.4 days. The solid lines in Fig. 2 represent the final selection criteria for IC79 where events above the lines constitute the final sample. The final selection criteria for the IC86 sample are defined as follows:

$$\log_{10} \text{NPE} \geq \begin{cases} 4.8 & \cos \theta < 0.075 \\ 4.8 + 1.6 \sqrt{1 - \left(\frac{1.0 - \cos \theta}{0.925}\right)^2} & \cos \theta \geq 0.075. \end{cases} \quad (1)$$

The resulting neutrino effective areas, the equivalent area at the Earth’s surface in which neutrinos are detected with 100% efficiency, averaged over the two-year period from May 2010 to May 2012 taking into account the different detector configurations, is shown in Fig. 3. The effective areas are given for each neutrino flavor averaged over 4π solid angle. They show that the analysis starts to be sensitive in the energy region around 1 PeV with its sensitivity rapidly increasing with energy. The effective area is larger for ν_e than ν_μ or ν_τ below 10 PeV which illustrates the sensitivity of the present analysis to cascade events in this energy region.

The expected numbers of background events in the final sample for the 615.9 day livetime from atmospheric muons and neutrinos from decays of pions and kaons are 0.038 ± 0.004 (stat) $^{+0.021}_{-0.038}$ (syst) and 0.012 ± 0.001 (stat) $^{+0.010}_{-0.007}$ (syst), respectively. Compared to previous analyses, the utilized atmospheric neutrino flux models [15] accommodate an improved parametrization of the primary cosmic-ray spectrum and composition which accounts now for the “knee” in the cosmic-ray spectrum. Adding prompt atmospheric neutrinos from decays of charmed mesons assuming the model in [16] with the improved cosmic-ray spectrum modeling, the total number of background events increases

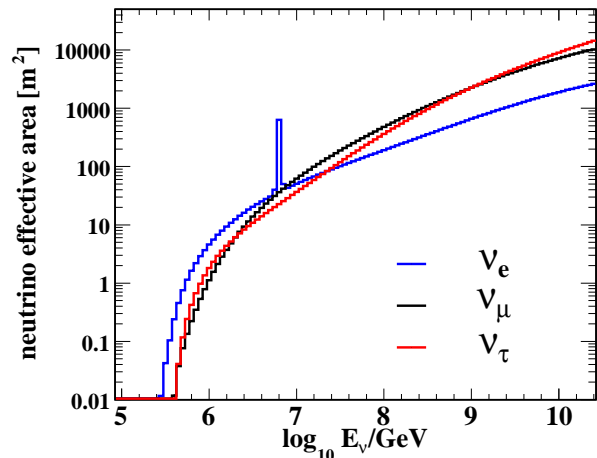


FIG. 3. The average neutrino effective area in the present analysis for a 4π isotropic flux, 615.9 days livetime, and the IC79 and IC86 string configurations. Exposure of the sample used in this analysis is obtained by multiplying the effective area with the livetime and 4π solid angle. The sharp-peaked structure for $\bar{\nu}_e$ at 6.3 PeV is due to the Glashow resonance [14].

to 0.082 ± 0.004 (stat) $^{+0.041}_{-0.057}$ (syst). We note that the charmed meson production cross-section used here is uncertain to a large degree. Theoretical uncertainties in our baseline model [16] which uses perturbative-QCD calculations are included in the background estimation. In addition, potential non-perturbative contributions, such as intrinsic charm in nuclei [17] or from the gluon density at small x , could lead to significantly larger cross sections and hence higher prompt neutrino fluxes. The IceCube limits on the prompt flux are about a factor of four higher than the baseline model [18].

The main systematic uncertainties on the backgrounds are from the measurement of NPE and from uncertain-

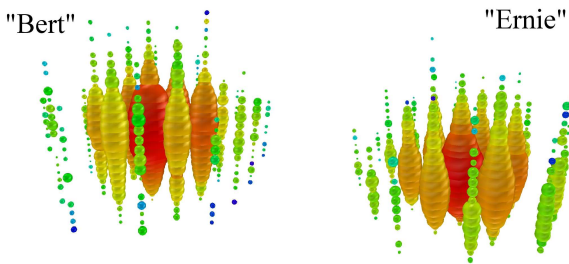


FIG. 4. The two observed events from August 2011 (left panel) and January 2012 (right panel). Each sphere represents a DOM. Colors represent the arrival times of the photons where red indicates early and blue late times. The size of the spheres is a measure for the recorded number of photoelectrons.

ties in the cosmic-ray flux. Uncertainties in the expected number of background events are estimated by varying the associated parameters in the simulation. The two dominant sources of experimental uncertainties are the absolute DOM sensitivity and the optical properties of the ice which contribute with (+43%, -26%) and (+0%, -42%), respectively. Uncertainties in the cosmic-ray flux models are dominated by the primary composition (+0%, -37%) and the flux normalization (+19%, -26%). The theoretical uncertainty in the neutrino production from charm decay [16] relative to the total background is (+13%, -16%). The systematic uncertainties are assumed to be evenly distributed in the estimated allowed range and are summed in quadrature.

The atmospheric muon and neutrino background events are simulated independently. However, at higher energies, events induced by downward-going atmospheric neutrinos should also contain a significant amount of atmospheric muons produced in the same air shower as the neutrino [19]. Since these events are reconstructed as downward-going, they are more likely to be rejected with the higher NPE cut in this region. Thus, the number of simulated atmospheric neutrino background events is likely overestimated in the current study.

After unblinding the 615.9 days of data, we observe two events that pass all the selection criteria. The hypothesis that the two events are fully explained by atmospheric background including the baseline prompt atmospheric neutrino flux [16] has a p-value of 2.9×10^{-3} (2.8σ). This value takes the uncertainties on the expected number of background events into account by marginalizing over a flat error distribution. Since the prompt component has large theoretical uncertainties we have also studied how much our baseline prompt component has to be enlarged so that the two events can be explained as atmospheric neutrinos: obtaining two or more events with a probability of 10% would require a prompt flux that is about 15 times higher than the central value of our perturbative-

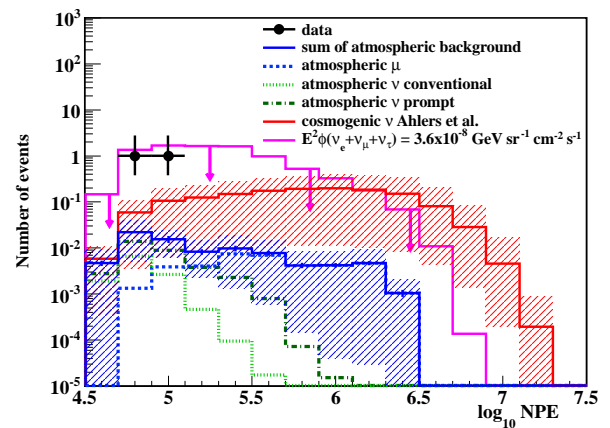


FIG. 5. Event distributions for 615.9 days of livetime at final cut level as a function of \log_{10} NPE. The black points represent the experimental data. The error bars on the data points show the Feldman-Cousins 68% confidence interval [20]. The solid blue line marks the sum of the atmospheric muon (dashed blue), conventional atmospheric neutrino (dotted light green) and the baseline prompt atmospheric neutrino (dot-dashed green) background. The error bars on the line and the shaded blue region are the statistical and systematic uncertainties, respectively. The red line represents the prediction of a cosmogenic neutrino model (Ahlers *et al.* [21]) with the model uncertainty indicated by the shaded region. The magenta line represents a power-law flux which follows E^{-2} up to an energy of 10^9 GeV with an all-flavor normalization of $E^2 \phi_{\nu_e + \nu_\mu + \nu_\tau} = 3.6 \times 10^{-8} \text{ GeV sr}^{-1} \text{ s}^{-1} \text{ cm}^{-2}$, which is the integral upper limit obtained in a previous search in a similar energy range [12]. Signal neutrino model fluxes are summed over all neutrino flavors, assuming a flavor ratio of $\nu_e : \nu_\mu : \nu_\tau = 1 : 1 : 1$.

QCD model. This contradicts our current limit on the prompt flux which would allow for not more than 3.8 times the central value at 90% C.L. [18].

The two events are shown in Fig. 4. Both events are from the IC86 sample, but would have also passed the selection criteria of the IC79 sample. The spherical photon distributions of the two events are consistent with the pattern of Cherenkov photons from particle cascades induced by neutrino interactions within the IceCube detector. There are no indications for photons from in-coming or out-going muon or tau tracks. Hence, these events are most likely induced by either CC interactions of electron neutrinos or NC interactions of electron, muon or tau neutrinos. CC interactions of tau neutrinos induce tau leptons with mean decay lengths of about 50 m at these energies [22]. The primary neutrino interaction and the secondary tau decay initiate separate cascades which in a fraction of such events lead to an observable double-peak structure in the recorded waveforms. The two events do not show a significant indication of such a signature. Figure 5 shows the final-cut NPE distributions for the experimental data, several signal models and background

Monte Carlo simulations. The two events are found near the NPE threshold of the analysis. These two events are consistent with a previous upper limit by IceCube [12] on an unbroken E^{-2} flux (Fig. 5, histogram with downward arrows), while a flux corresponding to this upper limit predicts about 10 events above the NPE cut.

For the dedicated reconstruction of the two events, a maximum-likelihood fit is utilized. The likelihood is the product of the Poisson probabilities to observe the recorded number of photo-electrons in a given time interval and DOM for a cascade hypothesis which depends on the interaction vertex, deposited energy and direction. Here, the time of the first hit mainly determines the vertex position and the recorded NPE plays a dominant role in estimating the deposited energy. The hit information used in the reconstruction is extracted from an unfolding procedure of the waveforms. The open circles in Fig. 1 indicate the strings closest to the reconstructed vertex positions. The reconstructed deposited energies of the two cascades are 1.04 PeV and 1.14 PeV, respectively, with a combined statistical and systematic uncertainty of $\pm 15\%$ each. The errors on the deposited energies are obtained by simulating cascade events in the vicinity of the reconstructed energies and vertices. The study is specifically performed on each event and the larger of the two event uncertainties is cited for both events. Thus, the error associated with the two events is different from errors for other cascade events observed in IceCube [23]. Since there is no absolute energy standard with adequate precision at these energies, the energy scale is derived from simulations based on measured ice properties and PMT efficiencies which are assured by measurements of atmospheric muons. The main sources of the systematic uncertainty on the reconstructed energies are the absolute DOM sensitivity and the optical properties of the ice [24]. The effect of the latter is estimated to be $+9\%$ and -5% and is obtained by varying the scattering and absorption coefficients for the photon propagation by 10% . The reconstruction algorithm includes variations of the scattering and absorption coefficients with depth (ice layers) [25]. The effect of a possible azimuthal anisotropy of the ice parameters and a tilt of the ice layers on the reconstructed energies is estimated to be $\pm 5\%$. The uncertainty on the absolute DOM sensitivity is $\pm 10\%$ which scales linearly with the uncertainty on the reconstructed deposited energy. The suppression of bremsstrahlung and pair production due to the LPM effect [26] is negligible in this energy range. The properties of the two observed events are summarized in Tab. I.

The reconstructed energy corresponds to the energy of the incoming neutrino if the observed cascade is the result of a CC interaction of electron or anti-electron neutrino in deep-inelastic scattering, as in this case the total neutrino energy is deposited near the interaction vertex [27]. On the other hand, NC interactions of neutrinos of any flavor or interactions of electron anti-neutrinos via the

events	“Bert”	“Ernie”
date (GMT)	August 8, 2011	January 3, 2012
NPE	7.0×10^4	9.6×10^4
number of recorded DOMs	312	354
reconstructed deposited energy (PeV)	1.04 ± 0.16	1.14 ± 0.17
reconstructed z vertex (m)	122 ± 5	25 ± 5

TABLE I. List of characteristics of the two observed events. The vertex z positions are with respect to the center of the IceCube detector at a depth of 1948 m.

Glashow resonance at 6.3 PeV [14] with outgoing leptons induce cascades which carry only a fraction of the neutrino energy. However, given the reconstructed energies, the observed cascades are unlikely to originate from the Glashow resonance as only about 10% of these interactions will deposit 1.2 PeV or less in the detector in cascade-like signatures.

The two PeV neutrino events observed in two years of data taken with the IceCube neutrino telescope may be a first hint of an astrophysical high-energy neutrino flux. However, given the yet rather moderate significance of 2.8σ with respect to the expected atmospheric background and the large uncertainties on its prompt component, a firm astrophysical interpretation requires more data in combination with analyses in other detection channels and energy ranges.

We acknowledge the support from the following agencies: U.S. National Science Foundation-Office of Polar Programs, U.S. National Science Foundation-Physics Division, University of Wisconsin Alumni Research Foundation, the Grid Laboratory Of Wisconsin (GLOW) grid infrastructure at the University of Wisconsin - Madison, the Open Science Grid (OSG) grid infrastructure; U.S. Department of Energy, and National Energy Research Scientific Computing Center, the Louisiana Optical Network Initiative (LONI) grid computing resources; Natural Sciences and Engineering Research Council of Canada, Compute Canada and Compute West High Performance Computing; Swedish Research Council, Swedish Polar Research Secretariat, Swedish National Infrastructure for Computing (SNIC), and Knut and Alice Wallenberg Foundation, Sweden; German Ministry for Education and Research (BMBF), Deutsche Forschungsgemeinschaft (DFG), Helmholtz Alliance for Astroparticle Physics (HAP), Research Department of Plasmas with Complex Interactions (Bochum), Germany; Fund for Scientific Research (FNRS-FWO), FWO Odysseus programme, Flanders Institute to encourage scientific and technological research in industry (IWT), Belgian Federal Science Policy Office (Belspo); University of Oxford, United Kingdom; Marsden Fund, New Zealand; Australian Research Council; Japan Society for Promotion of Science (JSPS); the Swiss National Science Foun-

ation (SNSF), Switzerland.

-
- * Physics Department, South Dakota School of Mines and Technology, Rapid City, SD 57701, USA
- † Los Alamos National Laboratory, Los Alamos, NM 87545, USA
- ‡ Corresponding author: aya@hepburn.s.chiba-u.ac.jp (A. Ishihara)
- § also Sezione INFN, Dipartimento di Fisica, I-70126, Bari, Italy
- ¶ Department of Physics, Sungkyunkwan University, Suwon 440-746, Korea
- ** NASA Goddard Space Flight Center, Greenbelt, MD 20771, USA
- [1] A. Achterberg *et al.* (IceCube Collaboration), *Astropart.Phys.* **26**, 155 (2006).
- [2] R. Abbasi *et al.* (IceCube Collaboration), *Astropart.Phys.* **35**, 615 (2012).
- [3] R. Abbasi *et al.* (IceCube collaboration), *Nucl. Instrum. Meth.* **A601**, 294 (2009).
- [4] R. Abbasi *et al.* (IceCube collaboration), *Nucl. Instrum. Meth.* **A618**, 139 (2010).
- [5] R. Abbasi *et al.* (IceCube Collaboration), *Phys. Rev.* **D82**, 072003 (2010).
- [6] S. Yoshida and M. Teshima, *Prog.Theor.Phys.* **89**, 833 (1993), the model with the source evolution $(z_{max} + 1)^m$ with $m = 4$ extending to $z_{max} = 4.0$.
- [7] D. Heck *et al.*, *CORSIKA: A Monte Carlo Code to Simulate Extensive Air Showers* (Report FZKA 6019, Forschungszentrum Karlsruhe, 1998).
- [8] E.-J. Ahn, R. Engel, T. K. Gaisser, P. Lipari, and T. Stanev, *Phys.Rev.* **D80**, 094003 (2009).
- [9] J. Ahrens *et al.*, *Nucl. Instrum. Meth.* **524**, 169 (2004).
- [10] P. Huber, *Robust Statistics* (Wiley, New York, 1981).
- [11] M. Wellons *et al.*, “Robust statistics in muon reconstruction,” (2013), proceedings of the 33rd International Cosmic Ray Conference (ICRC2013), to be published.
- [12] R. Abbasi *et al.* (IceCube Collaboration), *Phys.Rev.* **D83**, 092003 (2011).
- [13] G. Hill and K. Rawlins, *Astropart. Phys.* **19**, 393 (2003).
- [14] S. L. Glashow, *Physical Review* **118**, 316 (1960).
- [15] T. K. Gaisser, *Astropart.Phys.* **35**, 801 (2012).
- [16] R. Enberg, M. H. Reno, and I. Sarcevic, *Phys.Rev.* **D78**, 043005 (2008).
- [17] S. Brodsky *et al.*, *Phys. Lett. B* **93**, 451 (1980).
- [18] A. Schukraft (IceCube Collaboration), (2013), arXiv:1302.0127.
- [19] S. Schönert, T. K. Gaisser, E. Resconi, and O. Schulz, *Phys. Rev. D* **79**, 043009 (2009).
- [20] G. J. Feldman and R. D. Cousins, *Phys. Rev. D* **57**, 3873 (1998).
- [21] M. Ahlers, L. A. Anchordoqui, M. Gonzalez-Garcia, F. Halzen, and S. Sarkar, *Astropart.Phys.* **34**, 106 (2010).
- [22] D. Cowen (IceCube Collaboration), *J.Phys.Conf.Ser.* **60**, 227 (2007).
- [23] R. Abbasi *et al.* (IceCube Collaboration), *Phys. Rev. D* **84**, 072001 (2011).
- [24] M. Aartsen *et al.*, *Nucl. Instrum. Meth.* **711**, 73 (2013).
- [25] J. Lundberg *et al.*, *Nucl. Instrum. Meth.* **A581**, 619 (2007).
- [26] L. Gerhardt and S. R. Klein, *Phys. Rev. D* **82**, 074017 (2010).
- [27] The energy reconstruction assumes that all light emission originates from an electromagnetic shower. A hadronic cascade with the same light yield as the observed events would on average have an about 10% higher energy.